Quaternary Research

doi:10.1017/qua.2019.25

Iron Age landscape changes in the Benoué River Valley, Cameroon

David K. Wright[a,b]*, Scott MacEachern[c], Stanley H. Ambrose[d], Jungyu Choi[a], Jeong-Heon Choi[e], Carol Lang[f], Hong Wang[g,b]

[a]Department of Archaeology, Conservation and History, University of Oslo, N-0315 Oslo, Norway
[b]State Key Laboratory of Loess and Quaternary Geology, Institute of Earth Environment, Chinese Academy of Sciences, Xi'an, 710061, China
[c]Division of Social Science, Duke Kunshan University, Kunshan, Jiangsu, 215316, China
[d]Department of Anthropology, University of Illinois, Urbana, Illinois, 61801, USA
[e]Department of Earth and Environmental Sciences, Korea Basic Science Institute, Chungbuk, 28119, South Korea
[f]Department of Archaeology, University of York, York, YO1 7EP, United Kingdom
[g]Interdisciplinary Research Center of Earth Science Frontier, Beijing Normal University, Beijing 100875, China
*Corresponding author E-mail address: daudi.wright@gmail.com (D.K. Wright).

(Received August 30, 2018; Accepted April 18, 2019)

Abstract

The introduction of agriculture is known to have profoundly affected the ecological complexion of landscapes. In this study, a rapid transition from C_3 to C_4 vegetation is inferred from a shift to higher stable carbon ($^{13}C/^{12}C$) isotope ratios of soils and sediments in the Benoué River Valley and upland Fali Mountains in northern Cameroon. Landscape change is viewed from the perspective of two settlement mounds and adjacent floodplains, as well as a rock terrace agricultural field dating from 1100 cal yr BP to the recent past (<400 cal yr BP). Nitrogen ($^{15}N/^{14}N$) isotope ratios and soil micromorphology demonstrate variable uses of land adjacent to the mound sites. These results indicate that Early Iron Age settlement practices involved exploitation of C_3 plants on soils with low $\delta^{15}N$ values, indicating wetter soils. Conversely, from the Late Iron Age (>700 cal yr BP) until recent times, high soil and sediment $\delta^{13}C$ and $\delta^{15}N$ values reflect more C_4 biomass and anthropogenic organic matter in open, dry environments. The results suggest that Iron Age settlement practices profoundly changed landscapes in this part of West Africa through land clearance and/or utilization of C_4 plants.

Keywords: Holocene; Savanna; West Africa; Agriculture; Anthropogenic soils; Niche construction; Soil carbon; Nitrogen isotopes

INTRODUCTION

The spread of agriculture across Africa is argued to have had significant impacts on its ecological systems, which include forest fragmentation and the presence of more open landscapes (for recent reviews, see Oslisly et al., 2013; Marchant et al., 2018; Marshall et al., 2018). Although human niche construction occurred during the Pleistocene (Ambrose, 2010; Crowther et al., 2018), the scope and scale of anthropogenic environmental alteration has accelerated since food production began (Boivin et al., 2016). Historical and archaeological records show that the per capita land use by pre-Industrial Revolution farmers exceed that of modern people to obtain equivalent amounts of food (Ruddiman, 2013). Gauging the impacts of agriculture on ambient prehistoric biodiversity can be difficult because taphonomic effects and imprecise lines of proxy evidence can confound interpretation of anthropogenic versus natural ecological dynamics (Foley et al., 2013). Ultimately, more ecological records that focus on the scope and scale of impacts associated with prehistoric agricultural practices are needed to provide clearer context for the interdependence of current human-ecological systems.

The region of western Africa lies south of the Sahara (approximately 15°N), north of the Gulf of Guinea, and west of 15°E. It is the area of original domestication for several important African crop species, including sorghum (*Sorghum bicolor*), African rice (*Oryza glaberrima*), and pearl millet (*Pennisetum glaucum*). Some of these crops ultimately spread across most of sub-Saharan Africa by ca. 1800 yr ago (Kay and Kaplan, 2015; Lander and Russell, 2018). However, there are significant gaps in our understanding of the ecological contexts of domestication for all of these plants (Manning et al., 2011). Recent attention has focused on the spread of agriculture in the northern part of Central Africa. There are two competing sets

Cite this article: Wright, D. K., MacEachern, S., Ambrose, S. H., Choi, J., Choi, J.-H., Lang, C., Wang, H. 2019. Iron Age landscape changes in the Benoué River Valley, Cameroon. *Quaternary Research* 92, 323–339. https://doi.org/10.1017/qua.2019.25

of explanations for that spread: one holds that drier monsoon conditions after 2500 yr provided opportunities for agricultural colonists to plant in newly opened areas where tropical forest previously stood (Maley, 2002; Maley et al., 2012; Lézine et al., 2013; Bostoen et al., 2015; Grollemund et al., 2015; Clist et al., 2018), while the other argues that humans cleared forests for fuel to produce iron and facilitate an agricultural economy (Bayon et al., 2012; Morin-Rivat et al., 2014; Kay and Kaplan, 2015; Garcin et al., 2018). Ultimately, understanding landscape formation processes within the context of domestication is critical to determine the dependence of ecological systems on specific land management practices. In addition, the debate cited above highlights the increasing interest in the degree to which natural ecosystems were altered to facilitate the expansion into different environments (see also Boivin et al., 2016). The lack of knowledge from adjacent regions at different points in time means, however, that this research in the northern parts of the tropical forest cannot be placed in broader comparative contexts, whether those be environmental or cultural.

To resolve such issues, multiple lines of proxy evidence from well-dated archaeological sites can provide a broad environmental context for the arrival of anthropogenic effects into a region concurrent with domestication. Concentrations of nutrients on the landscape at the hectare scale in settlements with livestock corrals systematically increase floral microhabitat diversity that can be quantified with satellite imagery; floral and soil transect surveys; and sedimentary, chemical, and isotopic analyses of soils (Marshall et al., 2018). Other agricultural and land use practices, such as coppicing, burning of pastures and agricultural fields, grazing livestock, and cultivation, change soil nutrient composition in ways that are not always obvious from a "macro-view" of site formation processes. Techniques such as soil micromorphology combined with geochemical reconstruction offer a comparative before-and-after perspective on the qualitative and quantitative impacts of human niche construction on the environment (Meharg et al., 2006; Ackermann et al., 2014; Solís-Castillo et al., 2015). Geochronometry of both depositional and organic facies using optically stimulated luminescence (OSL) and radiocarbon (^{14}C) dating, respectively, provides a temporal framework of the timing and rates of anthropogenic environmental change. Chronologically constrained datasets can provide multiple lines of correlative evidence to understand causal factors for landscape change. Using soil organic stable carbon ($\delta^{13}C$) and nitrogen ($\delta^{15}N$) isotopes and micromorphological analyses from dated contexts, this paper presents evidence from the Benoué River Valley and adjacent highlands in northern Cameroon for an anthropogenically induced turnover in soil isotopic composition associated with artificial tell mound construction beginning 1100 yr.

BACKGROUND OF THE STUDY AREA

The project area is located in northern Cameroon, in the lowland trough of the Yola Rift, draining waters from the Mandara Mountains to the north and Adamaoua Plateau to the south (Fig. 1). A Sudanian woodland to grassy woodland community characterizes the historic habitat of the region, with varying proportions of grasses (White, 1983). Woodland biomes are dominated by trees with open canopies, allowing sufficient light to support an understory of up to 40% heliophilous (sun-loving) C_4 grasses and shrubs. Examples of environments that are minimally impacted by human activities are found nearby in the Benoué National Park, where savanna woodlands are characterized by dominant tree taxa, including *Combretum*, *Terminalia*, and *Acacia* (White, 1983). The principle vegetation types are highly dependent on water availability. Hydrophilic closed woodlands with sparse understory C_3 grasses are found primarily in the river valleys, with deciduous woodlands in the upland regions. Riparian forest and closed woodlands have higher tree densities, with sparse grasses (~3%) in the understory (White, 1983; Stark and Hudson, 1985).

The greater Lake Chad region was occupied exclusively by hunter-gatherers until 4000 yr, after which farming and herding economies entered the region (MacEachern, 2012; Maley and Vernet, 2015). By 2400–2200 cal yr BP, shaft furnaces for producing iron are found in sub-Saharan western Africa (Killick, 2015), and Iron Age farmers were widely distributed across the region by 2000 yr (Russell et al., 2014; Bostoen et al., 2015). Iron Age settlement in mounds adjacent to the Benoué River Valley is traced from at least 1500 cal yr BP (David, 1981). By 1000 cal yr BP, people were planting sorghum (*Sorghum* sp.) and finger millet (*Eleusine coracana*), raising cattle (*Bos taurus*), goats (*Capra hirca*), and sheep (*Ovis aries*), and fishing from local streams (David, 1981).

Humans are hypothesized to be significant agents of regional landscape change in western Africa since the introduction of plant cultivation at ca. 4000 yr (Kahlheber and Neumann, 2007; Kay and Kaplan, 2015; Garcin et al., 2018), but the degree to which natural climate variability versus anthropogenic clearing was the driving factor of landscape change remains an open question. In order to examine the pace of ecological succession within the context of the emergence of agricultural economies, the present study presents soil stable isotopic and micromorphological evidence to better understand past human impacts on floral habitats and landscape change on a subregional scale.

STABLE ISOTOPES OF SOIL AS ECOLOGICAL PROXIES

The $\delta^{13}C$ value of soil organic carbon is closely correlated with that of standing plant biomass, and has been widely used to reconstruct proportions of trees to grasses in tropical African environments (Ambrose and Sikes, 1991; Delègue et al., 2001; Runge, 2002; WoldeGabriel et al., 2009; Wang et al., 2010). Trees, shrubs, and most leafy herbaceous dicotyledonous plants, along with some shade- and cold-tolerant grasses (including *Oryza* rice and wheat), fix atmospheric carbon dioxide (CO_2) using the C_3 photosynthetic pathway to produce a three-carbon molecule in the first step of photosynthesis. This biochemical process discriminates strongly against

https://doi.org/10.1017/qua.2019.25 Published online by Cambridge University Press

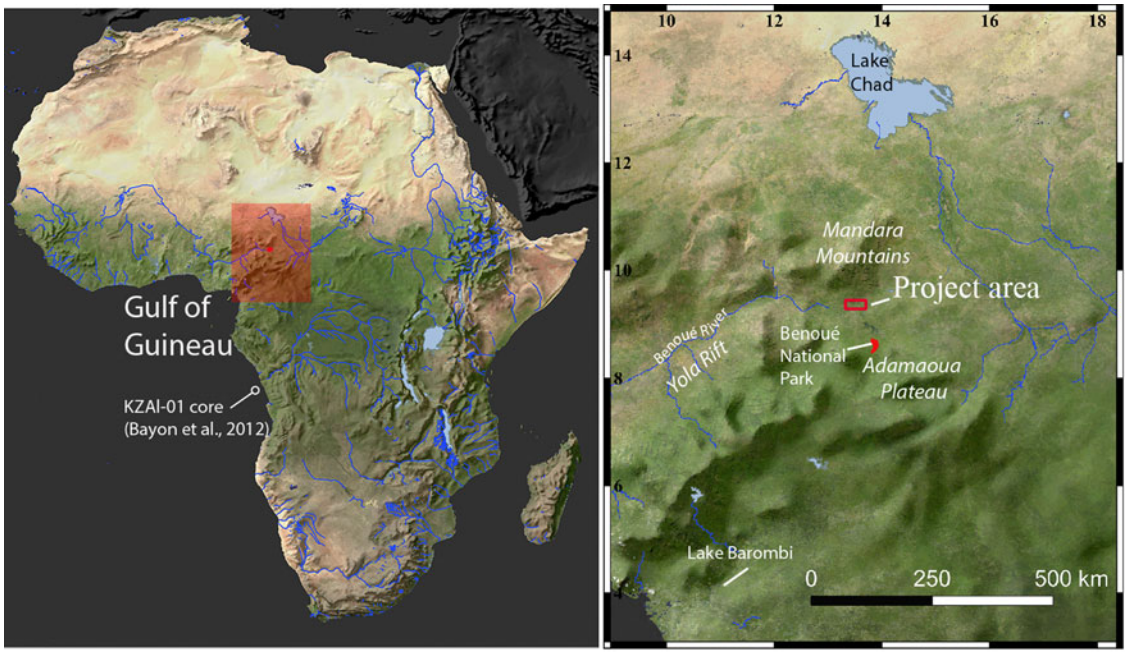

Figure 1. (color online) Location of the study area. Numbers on the horizontal (x-) axis are degrees radian east of prime meridian and numbers on the vertical (y-) axis are degrees radian north of the equator relative to the WGS84 geodetic datum.

$^{13}CO_2$, so C_3 plants have consistently lower $^{13}C/^{12}C$ ratios, with $\delta^{13}C$ values lower than −23‰ versus the Vienna Pee Dee Belemnite (VPDB) standard (Kim et al., 2015). Conversely, most tropical grasses (including sorghum, millets, *Digitaria* sp., African rice, and savanna grasses), sedges (e.g., papyrus), and a few broadleaf herbaceous species that are adapted to strong sunlight and high temperatures use the C_4 pathway, which discriminates much less against the heavier isotope, and have $\delta^{13}C$ values consistently higher than −16‰ (O'Leary, 1988). Average $\delta^{13}C$ values of C_3 plants are approximately −27‰, and would have been approximately −26‰ in the pre-Industrial era. C_4-plant $\delta^{13}C$ values would have been approximately −12‰ (Kohn, 2010). Soil organic matter decomposition is accompanied by an enrichment of ~1‰ (Natelhoffer and Fry, 1988), so soils with 100% C_3 and C_4 plant biomass have average $\delta^{13}C$ values of approximately −25 and −11‰, respectively (Ambrose and Sikes, 1991).

Soil nitrogen isotope ratios in natural ecosystems are inversely correlated with rainfall and temperature, and can be used as a general index of aridity (Ambrose, 1991). Plant and soil $\delta^{15}N$ values are also consistently higher in anthropogenic sediments (Commisso and Nelson, 2006), particularly in areas where domestic animals are corralled (Shahack-Gross et al., 2008; Marshall et al., 2018) and during natural leaf litter and soil organic matter decomposition (Natelhoffer and Fry, 1988; Högberg, 1997).

METHODS

Archaeological survey and site documentation

In order to investigate human-landscape interactions within the context of Iron Age settlement of West Africa, archaeological research was undertaken northeast of Garoua, Cameroon, in June and July 2014 (Fig. 2). An archaeological survey was undertaken to revisit sites initially investigated by David (1968, 1981) along the Benoué River and to collect samples for dating, micromorphology, sedimentology, and geochemistry. Documentation of site locations and attributes were made using a Trimble XH GPS unit. Details of project objectives and survey methods have been previously published in Wright et al. (2017).

The primary focus of site documentation was on the site of Langui-Tschéboua (GRA-4, 9.32°N, 13.62°E; Wright et al., 2017), an anthropic mound bisected by a seasonal stream. The mound and adjacent field site was cleaned and profiled, and the stratigraphic positions of soils and sediments across the exposure were systematically mapped. The mound was subjected to three-dimensional mapping to record lateral and vertical distribution of material culture remains. Archaeological features were documented in the site fill, and lithological units traced across the site area and to the surrounding terrace surface exposures. Site documentation extended to the adjacent terrace regions to connect mound activity areas with possible concurrent agricultural activity areas. The alluvial terraces and outlying depositional contexts were classified as "off-site" areas relative to "on-site" areas, which were anthropogenic mounds in the lowlands and artificial terraces in the uplands. By separating these contexts, we sought to constrain the spatial and temporal scale of anthropogenesis as agricultural practices spread into the region.

Sediment cores were extracted using a percussion auger from the lower terrace of the Benoué River floodplain adjacent to the site of Bé (9.30°N, 13.66°E). Samples from the Bé mound were collected 14.2 m northwest of David's (1981)

https://doi.org/10.1017/qua.2019.25 Published online by Cambridge University Press

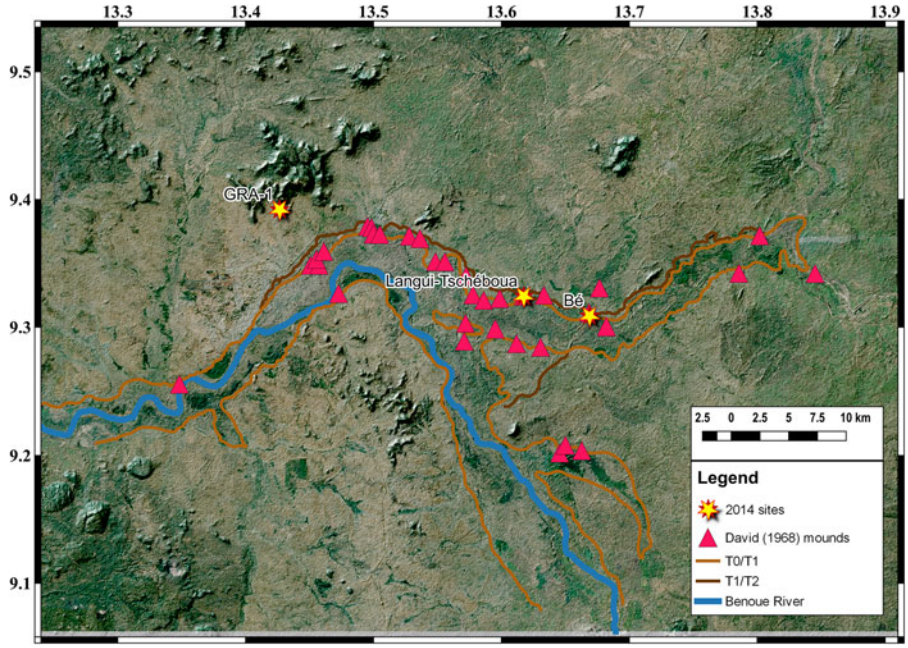

Figure 2. (color online) Benoué River Valley mounds (David, 1968), archaeological sites, and alluvial terraces documented in 2014. Refer to Figure 1B for the project area location.

excavation unit and achieved a depth of 204 cm below the modern ground surface (CAM-BE-Rock 8). A percussion auger core (CAM-BE-Rock 7) was also collected from the field adjacent to the main mound and measured 130 cm deep.

Site GRA-1 (9.40°N, 13.44°E), located in the Fali Mountains, was discovered during the 2014 field season. This is a rock terrace agricultural field with undecorated ceramics on the ground surface. The site was mapped with a GPS unit and samples were collected from two contexts: a soil pit excavated near the center of the site, and two auger cores located in upland swales. The soil pit was located in an area of high artifact concentration between artificial terraces constructed from stones. This pit was excavated to a depth of 35 cm below the modern ground surface, where bedrock or a boulder impeded further excavation into the subsoil. Charcoal was collected for radiocarbon dating and sediment samples for stable isotopic reconstruction were extracted from both depositional units.

Two percussion auger sample sets were collected from swale depressions within and adjacent to the site. Core CAM-GRA1-Rock 6 was augered to a depth of 100 cm below the ground surface within a rock-terraced portion of the site. The second core (CAM-GRA1-Rock 5) was augured to a depth of 60 cm in an off-site, upland swale vegetated with marsh grasses.

OSL dating

Seven sediment samples were collected from GRA-4 contexts for OSL dating. OSL dating determines the last time that sand grains were exposed to light via the accumulation of natural radiation energies (α- and β-particles, γ- and cosmic rays) in the defects of the crystal matrix of minerals (Aitken, 1998). Samples were collected using sample tubes (~4 cm in diameter and ~25 cm in length) that shield the sediments from light. When silicate-rich sediment is exposed to light with a wavelength of 470 nm in controlled laboratory circumstances, a photomultiplier tube counts the vacating electrons and experiments follow to estimate the time it took to accumulate the stored energy.

For Langui-Tschéboua, quartz grains with diameters of 180–250 μm were prepared in the laboratory using wet-sieving, acid treatments (10% HCl, 10% H_2O_2, and 40% HF), and density separation in sodium polytungstate at a specific gravity of 2.61, and were analyzed using a TL/OSL-DA-20 Risø reader. The single aliquot regeneration protocol (Murray and Wintle, 2000, 2003) was followed. The reconstructed total amount of stored energy, called the equivalent dose (D_e), was determined to be independent of the preheat temperatures between 250 and 295°C based on preheat plateau tests. The rates of radioactive decay within the mineral matrix environment, or dose rates (D_r), of the samples were estimated using a Canberra Broad Energy Germanium 5030 low-level high-resolution gamma spectrometer. OSL signals were measured based on aliquots composed of several tens of quartz grains (small aliquots), and the final ages were derived using the central age model (Galbraith et al., 1999; Galbraith and Roberts, 2012). Ages reported have a 0 datum being the year AD 2014, which was when the samples were collected and analyzed. Thus, there is an inherent 64-yr offset between the radiocarbon and OSL ages.

Radiocarbon dating

Charcoal samples were collected for radiocarbon dating at the Illinois State Geological Survey (ISGS), Prairie Research

https://doi.org/10.1017/qua.2019.25 Published online by Cambridge University Press

Institute, University of Illinois at Urbana-Champaign. Preparation of the samples followed the standard acid-base-acid pretreatment protocol, converted into CO_2, after which they were loaded into a graphite target for accelerated mass spectrometry (AMS) analyses. The University of California-Irvine AMS Radiocarbon Laboratory performed radiocarbon analysis in which counts of ^{12}C, ^{13}C, and ^{14}C were measured to determine the Libby half-life (5730 yr) by the $^{14}C/^{13}C$ and $^{14}C/^{12}C$ ratio of each sample, with corrections based on the $^{13}C/^{12}C$ ratio. The results were calibrated to 2-σ of statistical confidence corresponding to yr BP (AD 1950) using CALIB 7.1 program (Stuiver et al., 2019), which applies the INTCAL13 calibration curve (Reimer et al., 2013).

Micromorphology

Undisturbed soil samples were collected for micromorphological analysis. All water was removed from samples through acetone exchange. Samples were then impregnated using polyester "polylite 32032-00" resin. Impregnated soils were cured, sliced, bonded to a glass slide, and precision lapped to 30-µm thickness to produce a soil thin section. Following procedures laid out in the International Handbook for Thin Section Description (Bullock et al., 1985) and in Stoops (2003), soil properties were recorded semiquantitatively. Thin sections were analyzed using a Zeiss' AxioLab.A1 with rotary stage, plane polarized light, cross-polarized light, and oblique incident light. These instruments allow identification of microscopic features, such as mineral and organic components, pedofeatures, and burnt residues.

Soil carbon and nitrogen isotopes

Soil samples were prepared using methods described by Ambrose and Sikes (1991). Sediments were inspected with a low magnification stereomicroscope to identify pedogenic features, texture, structure, and anthropogenic and other inclusions (e.g., charcoal, bone, burnt soil, angular- to waterworn-clasts, carbonate nodules, and shell). Munsell colors (wet and dry) were recorded and samples were photographed on Munsell color chart pages. Samples were gently ground with ceramic mortars and pestles, to disaggregate soils, while leaving rock and mineral components intact, and sieved to pass through a 0.25-mm mesh geological sieve.

Samples of the <250-µm fraction weighing ~5 g were prepared for isotopic analysis by reaction with 1M HCl in 50 mL glass centrifuge tubes for 20 hours, beginning with one hour on a shaker table at ~1000 RPM, in order to remove carbonates. Intensity of reaction with HCl was noted after acid was initially added in order to qualitatively assess carbonate content. Samples were examined again after 20 hours to assess whether carbonates remained, as indicated by continued generation of gas bubbles. If reaction was incomplete, HCl treatment was repeated. After HCl treatment, samples were agitated and centrifuged three times with distilled water. If pH was close enough to neutral to cause clays to remain suspended, a few drops of 1M HCl were added to flocculate clays, and then agitated and centrifuged again before decanting the supernatant. Samples were dried at 70°C in a gravity oven. Weight after drying was used to calculate weight loss due to removal of carbonates and other acid-soluble fractions. This is the carbonate-free whole soil fraction. Dried samples were homogenized inside their centrifuge tubes using a glass rod as a pestle. Mortars, pestles and all glassware used for wet chemistry were cleaned in an acid bath, then fired in a kiln at 520°C for two hours before use to oxidize carbon and prevent sample carbon cross-contamination.

For isotopic analysis, samples weighing 4–5 mg were sealed in tin foil capsules and combusted in a Carlo-Erba NC-2500 Elemental Analyzer to convert organic matter into purified CO_2 and N_2. The purified gases were then transferred to a Thermo-Finnegan Delta V Plus XL isotope ratio mass spectrometer to measure stable isotope ratios. In order to monitor precision, accuracy, and replicability of isotopic analyses and weight percent C and N, each set of samples analyzed included purified amino acid international reference standards USGS 40 and 41 at the beginning and end of each run.[1] Purified amino acid working standards (phenylalanine and serine) and thiourea were analyzed after every tenth soil sample. A total of 13 standards were included with each set of 35 samples. If average standard values differed consistently in one direction by approximately the same amount from consensus isotopic values, then the average deviation was used to correct sample values. Corrections ranged from 0.0‰ to less than 0.2‰ for the sample sets run in this study. The analytical precision of isotopic analysis of $\delta^{13}C$ and $\delta^{15}N$ was 0.1 and 0.2‰, respectively. The average difference of replicates of soil samples was 0.1 and 0.4‰ for $\delta^{13}C$ and $\delta^{15}N$, respectively. Weight percent C and N difference of replicates was 0.29 and 0.03%, respectively. Many soil samples had low N concentrations and others had concentrations below detection limits. Those with the lowest measurable N concentrations have higher proportions of background derived from air, which has a $\delta^{15}N$ value of 0‰. Therefore, the measured $\delta^{15}N$ vales reported here are likely lower than their actual $\delta^{15}N$ values. This may also account for higher differences in wt% N of replicates. Estimates of percent C_4 biomass are considered ± 10% due to the range of variation in C_3 and C_4 plant biomass, potential recent habitat change, and variation in $\delta^{13}C$ observed within modern sampling sites (Ambrose and Sikes, 1991).

Stable isotope values were statistically analyzed using the SIBER package in R (Jackson et al., 2011). SIBER generates standard ellipses of a distribution of data based on Bayesian random permutations of the actual data. Data were manually organized according to their geographic locations (called

[1]USGS40 and USGS41a purified L-Glutamic amino acid standards were analyzed at the beginning and end of each sequence of samples. For $\delta^{13}C$, average measured and expected values for USGS40 were −26.41 and −26.39‰, respectively. Measured average and expected values for USGS41a were 36.52 and −36.55‰, respectively (Qi et al., 2016). For $\delta^{15}N$, measured and expected values for USGS40 were −4.58 and −4.52‰, respectively. Measured and expected values for USGS41a were 46.79 and 47.55‰, respectively (Qi et al., 2016).

https://doi.org/10.1017/qua.2019.25 Published online by Cambridge University Press

groups) and communities were created based on on-archaeological site (on-site) and off-archaeological site (off-site) contexts. The creation of the ellipses was unsupervised and set to the 95% confidence interval.

RESULTS

Depositional context

Langui-Tschéboua is a mound feature bisected by the shifting course of the Mayo Badjouma seasonal stream (Fig. 3). The mound is constructed on top of a terrace, and is laterally exposed with fluvial scouring. The original elevated area of the mound was approximately 100 m along its short axis, although erosion of the site has been extensive. Fluvial incision is estimated to have removed approximately half of the total area of the mound, leaving a vertical scarp face, with continuous cultural deposits exposed to a depth of up to 5.4 m along the approximately 100-m exposure.

The stratigraphy and formation context of the Langui-Tschéboua mound has been previously published in Wright et al. (2017). In sum, there are two primary anthropogenic depositional components to the site of Langui-Tschéboua: the mound and adjacent fields. The mound is comprised of laminated lenses of sand, loamy sand and sandy loam with numerous artifacts eroding from the fill zones dating from between 1100 and 700 yr (Fig. 3, Tables 1 and 2). Bedding planes (cm-scale) were preserved in the alluvial substrate of the mound, but there were no depositional structures associated with the mound. Clay-rich lenses were identified in three units of the profile and ashy fill comprised five of the layers. Analysis of micromorphology confirmed the presence of ~2.5 m of discrete lenses of anthropogenic fill that were minimally compacted and variably rich in organic matter (Fig. 4a). Disseminated charcoal fragments and irregular contacts were also identified between layers (MM3A, MM5), but sample MM4 shows more diffuse, linear boundaries (Fig. 4b and c). The weak structure of the depositional features, poorly sorted and angular sediments, and OSL age of the mound fill that statistically overlaps with the alluvial substrate at 1-σ form the basis of interpretation that the mound was constructed as basket fill from the adjacent streambed (Wright et al., 2017). The adjacent agricultural fields are comprised of aggraded sand fining up to clay-dominant alluvium on top of which thin (<20 cm) soils develop. Micromorphological analysis finds evidence for burning of the terraces prior to soil formation, some evidence for trampling scars and redoximorphic features that typically occur in waterlogged settings.

The site of Bé was initially described by David (1968, 1981). Charcoal collected from lower and upper fill zones of the largest mound date from 1106 ± 33 ^{14}C yr

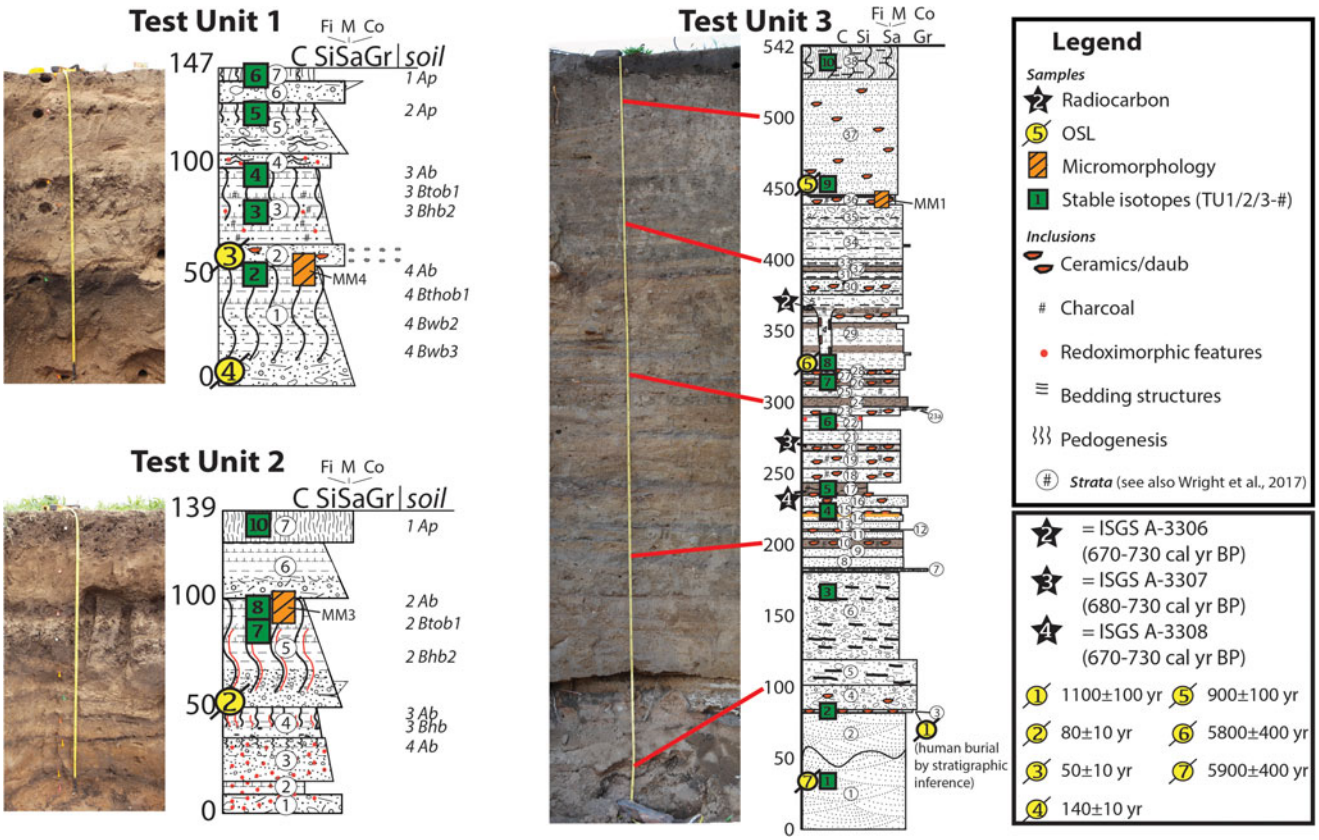

Figure 3. (color online) Langui-Tschéboua test units and sedimentologic profiles. Grain size classifications and abbreviations follow the United States Department of Agriculture taxonomy (Schoeneberger et al., 2012). A site plan map and locations of the profiled units are published in Wright et al. (2017).

https://doi.org/10.1017/qua.2019.25 Published online by Cambridge University Press

Table 1. Equivalent dose, dose rate, and optically stimulated luminescence ages of samples from Langui-Tschéboua, Cameroon.

Sample	Depth[a] (cm)	Water Content[b] (wt%)	^{238}U (Bq/kg)	^{226}Ra (Bq/kg)	^{232}Th (Bq/kg)	^{40}K (Bq/kg)	Dry beta[c] (Gy/ka)	Dry gamma[c] (Gy/ka)	Cosmic ray[d] (Gy/ka)	Total dose rate (Gy/ka)	D_e (Gy)	*n*	Age[e] (yr)	Over-dispersion (%)[f]	Context
CAM-GRA-14-OSL1	410	1.3	10.9 ± 3.3	11.0 ± 0.4	20.8 ± 1.2	776 ± 16	2.14 ± 0.08	0.95 ± 0.02	0.10 ± 0.01	3.14 ± 0.08	3.3 ± 0.2	24	1100 ± 100	23.3	Human burial fill
CAM-GRA-14-OSL2	88	15.5	21.1 ± 6.2	18.6 ± 0.6	65.8 ± 1.6	1075 ± 22	3.26 ± 0.12	1.79 ± 0.03	0.18 ± 0.02	4.43 ± 0.11	0.36 ± 0.03	21	80 ± 10	30.4	Fluvial terrace
CAM-GRA-14-OSL3	86	1.6	12.8 ± 5.5	14.2 ± 0.6	35.0 ± 1.5	1283 ± 23	3.50 ± 0.13	1.55 ± 0.03	0.18 ± 0.02	5.14 ± 0.13	0.23 ± 0.01	20	50 ± 10	9.0	Fluvial terrace
CAM-GRA-14-OSL4	147	8.1	7.8 ± 3.4	7.0 ± 0.4	16.3 ± 1.1	967 ± 20	2.55 ± 0.10	1.02 ± 0.02	0.16 ± 0.02	3.41 ± 0.09	0.49 ± 0.04	22	140 ± 10	35.3	Fluvial terrace
CAM-GRA-14-OSL5	96	3.0	18.9 ± 5.9	18.8 ± 0.5	34.3 ± 1.5	869 ± 17	2.52 ± 0.10	1.24 ± 0.02	0.18 ± 0.02	3.81 ± 0.10	3.5 ± 0.2	22	900 ± 100	23.2	Mound sediment
CAM-GRA-14-OSL6	221	1.8	9.5 ± 3.7	10.9 ± 0.5	17.9 ± 1.2	719 ± 17	1.98 ± 0.08	0.87 ± 0.02	0.14 ± 0.01	2.93 ± 0.08	17.1 ± 0.9	23	5800 ± 400	22.3	Mound sediment
CAM-GRA-14-OSL7	511	13.5	7.4 ± 3.0	8.4 ± 0.4	14.9 ± 1.0	607 ± 14	1.66 ± 0.07	0.72 ± 0.02	0.09 ± 0.01	2.14 ± 0.06	12.6 ± 0.6	24	5900 ± 300	17.4	Fluvial terrace

[a]Depths of samples are the vertical distance from the modern ground surface.
[b]Present water content.
[c]Data from high-resolution, low-level gamma spectrometer were converted to infinite matrix dose rates using conversion factors given in Olley et al. (1996).
[d]Cosmic ray dose rates were calculated using the equations provided by Prescott and Hutton (1994).
[e]Central age (±1-σ error) calculated to years before AD 2014 (yr).
[f]The overdispersion percentage of a D_e distribution is an estimate of the relative standard deviation from a central D_e value in context of a statistical estimate of errors (Galbraith et al., 1999; Galbraith and Roberts, 2012).

BP (930–1170 cal yr BP; P-1684) to 258 ± 39 ^{14}C yr BP (0–460 cal yr BP; P-1744; Lawn, 1973; Fig. 5). The deepest radiocarbon sample was collected 7 m below the modern ground surface, and the highest sample was collected at approximately 1 m below the modern ground surface. Based on the published chronology, the accumulation rate between 7 and 2 m below ground surface was approximately 1 m/125.8 yr. Alternating sand and clay laminates in the percussion auger core collected in 2014 (CAM-BE-Rock 8) were difficult to correlate precisely with the published stratigraphy (David, 1981). The floodplain core (CAM-BE-Rock 7) was comprised of mm- to cm-scale laminations of silty clays and clays with a silty intraclast at 90 cm below the modern ground surface. Laminates from this core were interpreted as evidence for multiple, episodic slackwater floodplain deposits.

At GRA-1, two depositional units were recorded from the shovel pit, which consisted of sandy loam overlying a lens of loamy sand (Fig. 6). A weak soil was documented within the sandy loam (0–19 cm below ground surface), which contained pottery and charcoal fragments dating to 795 ± 20 ^{14}C yr BP (680–730 cal yr BP; A-3309). From the on-site percussion auger core (CAM-GRA1-Rock 6), two primary depositional zones were observed with the substrate, consisting of a sandy clay loam below 70 cm, and a sandy loam from 0–70 cm below surface. Three buried soil horizons were documented in this core, the lowermost of which had charcoal inclusions. Redox mottles were observed in the middle soil. The off-site percussion auger core (CAM-GRA1-Rock 5) sedimentologic profile consisted of a fining-up sequence ranging from a sandy clay loam substrate to silt loam. Poorly sorted sediments indicate slowly aggrading colluvium that accumulated above a saprolite (decomposed bedrock). Topsoil formed in the silt loam sediments extending to approximately 15 cm below the modern ground surface.

Geochemistry of site formation

Paleosol and sediment carbon and nitrogen isotope ratios form two clusters (Fig. 7, Table 3). Higher δ^{13}C and δ^{15}N values characterize sediments from the later phase of mound settlement at Langui-Tschéboua and *karal*[2] fields at the site of Bé. Lower δ^{13}C and δ^{15}N were measured from the time period that precedes the Late Iron Age, those that occur at GRA-1, the late phase of mound settlement at Bé and floodplain soils at Langui-Tschéboua. The average δ^{13}C value of on-site and control samples was −17.9‰ with a range of −24.7 to −13.8‰. The average δ^{15}N value was +5.3‰ with a range of + 0.8 to + 12.4‰.

The δ^{13}C values from the mound at Langui-Tschéboua show an apparent shift from a C_3- to C_4-dominant floral

[2]*Karal* fields are locations of plant transhumance in which sorghum is planted in the sandy terraces in the rainy season and are transplanted to the clay-rich floodplain during the dry season until harvesting. Grassy, non-cultivated areas provide pasture for grazing livestock.

https://doi.org/10.1017/qua.2019.25 Published online by Cambridge University Press

Table 2. Radiocarbon ages from Langui-Tschéboua and Fali Mountains.

Sample (ISGS #)	Depth (cm)	Material	$\delta^{13}C$	^{14}C yr BP	cal yr BP[a, b]	Context
A-3306	189	Charcoal	−10.9	765 ± 20	670–730	Mound sediment
A-3307	270	Charcoal	−25.4	785 ± 20	680–730	Mound sediment
A-3308	307	Charcoal	−22.6	780 ± 25	670–730	Mound sediment
A-3309	9	Charcoal	−23.8	795 ± 20	680–730	Agricultural field

[a]Radiocarbon ages calibrated using CALIB7.1 (Reimer et al., 2013; Stuiver et al., 2019).
[b]Ages ± 2-σ error

habitat from the pre-Iron Age (5900 yr) to Iron Age (700 cal yr BP) contexts with a return to C_3 vegetation in the upper solum (Fig. 8). The basal sediments from the mound have the lowest $\delta^{13}C$ values of the mound sediments with an exponential-fit growth of $\delta^{13}C$ after human occupation correlating with the growth of the mound in the later periods of site formation. The control sample collected from the upper solum (modern "plow zone") of the mound has a value of −20.0‰, reflecting C_3 dominant vegetation. Similarly, samples collected in the upper 120 cm and 40 cm of Bé, which elevationally correlate with a radiocarbon age of 0–460 cal yr BP (P-1744), show lower $\delta^{13}C$ values (−16.7 and −18.0‰, respectively) relative to the off-site control samples collected in the adjacent fields (average = −14.1‰). The on-site GRA-1 sample collected from an archaeological soil dating to 700 cal yr BP in the Fali Mountains has a lower $\delta^{13}C$ value than all samples from Langui-Tschéboua (−20‰). However, the off-site control samples have even lower $\delta^{13}C$ values (average = −22.3‰).

The average $\delta^{13}C$ value from the off-mound control samples (excluding those extracted from the Bé floodplain) was −19.5‰, while the Bé floodplain samples averaged −14.8‰. The former set of controls indicates a C_3 environment (<50% grass), while the latter set reflects a C_4 grass-dominated habitat (70–90% grass). All off-site samples are presumed to come from contexts that date to within the last 1000 yr based on the preservation of laminate stratigraphy in the auger cores.

The $\delta^{15}N$ values cluster into two primary groups according to where they were collected: (1) values above the mean, from the mound sediments, the upper solum of an agricultural terrace at GRA-1, and the floodplain at Bé; and (2) values below the mean, from most of the off-site samples and those from GRA-1. The former group's $\delta^{15}N$ average is 7.5‰ and the latter group's average is 3.0‰. A linear regression (R function "lm") between $\delta^{13}C$ and $\delta^{15}N$ indicated a moderately positive correlation ($R^2 = 0.48$).

DISCUSSION

Analysis of soil and sedimentologic features of mounds in the Benoué River Valley demonstrate anthropogenic effects on the landscape ecology associated with the introduction of a subsistence economy based on plant cultivation (Fig. 9). Approximately 2.5 m of the Langui-Tschéboua mound sediment accumulation are interpreted as having occurred rapidly (within a timespan of approximately 60 yr based on the radiocarbon chronology of charcoal from the fill and micromorphology). In contrast, the settlement mound of Bé, as previously reported by David (1968, 1981) and Lawn (1973), appears to have progressively aggraded over centuries, although interpretation of the upper fill accumulation rate is hampered by imprecision in the correction for atmospheric concentrations of radiocarbon after 460 cal yr BP. The stable isotopic composition of mound sediments, however, shows significant statistical overlap in associated plant communities. These results indicate that, while formation processes may have differed for the mounds, the associated landscape processes were similar, particularly for the latter phases of occupation.

Closer examination of the available evidence demonstrates that there is a time-transgressive element to the transition from a C_3 to C_4 landscape. The initial occupation (ca. 1100 yr during the regional Middle Iron Age) of Langui-Tschéboua reflects only a modest (+1‰) shift in $\delta^{13}C$ relative to the middle Holocene floodplain deposits, but during the primary construction and occupation phase of the mound, the values shift more significantly (>5‰) toward C_4 vegetation (Fig. 8). We interpret this as evidence of an increasing scale of land clearance concurrent with the shift toward more agriculture and intensive human habitation of the mound. The final sample from the mound recovered 8 cm below the modern (farmed) ground surface seemingly suggests a stronger C_3 signature than the five samples collected below it. To support this interpretation, CORONA satellite imagery from the region taken in 1965 shows more extensive woodland than is currently present (Fig. 10). Less intensive recent habitation and cultivation of the Langui-Tschéboua mound site relative to the Iron Age appears to have promoted afforestation and the growth of C_3 vegetation.

The control samples and plow zone samples from the Langui-Tschéboua mound have more depleted $\delta^{13}C$ values, reflecting a C_3 environment, relative to the mound sediments that date to ca. 700 cal yr BP. OSL samples from this portion of the floodplain date to within the last 150 yr. Micromorphological analyses of the floodplain soils, however, do not consistently demonstrate intensive cultivation based on the presence of planting scars in thin sections. Based on observations of modern land-use practices, the lower floodplain is used for transhumant *karal* agriculture (Kenga et al., 2005;

https://doi.org/10.1017/qua.2019.25 Published online by Cambridge University Press

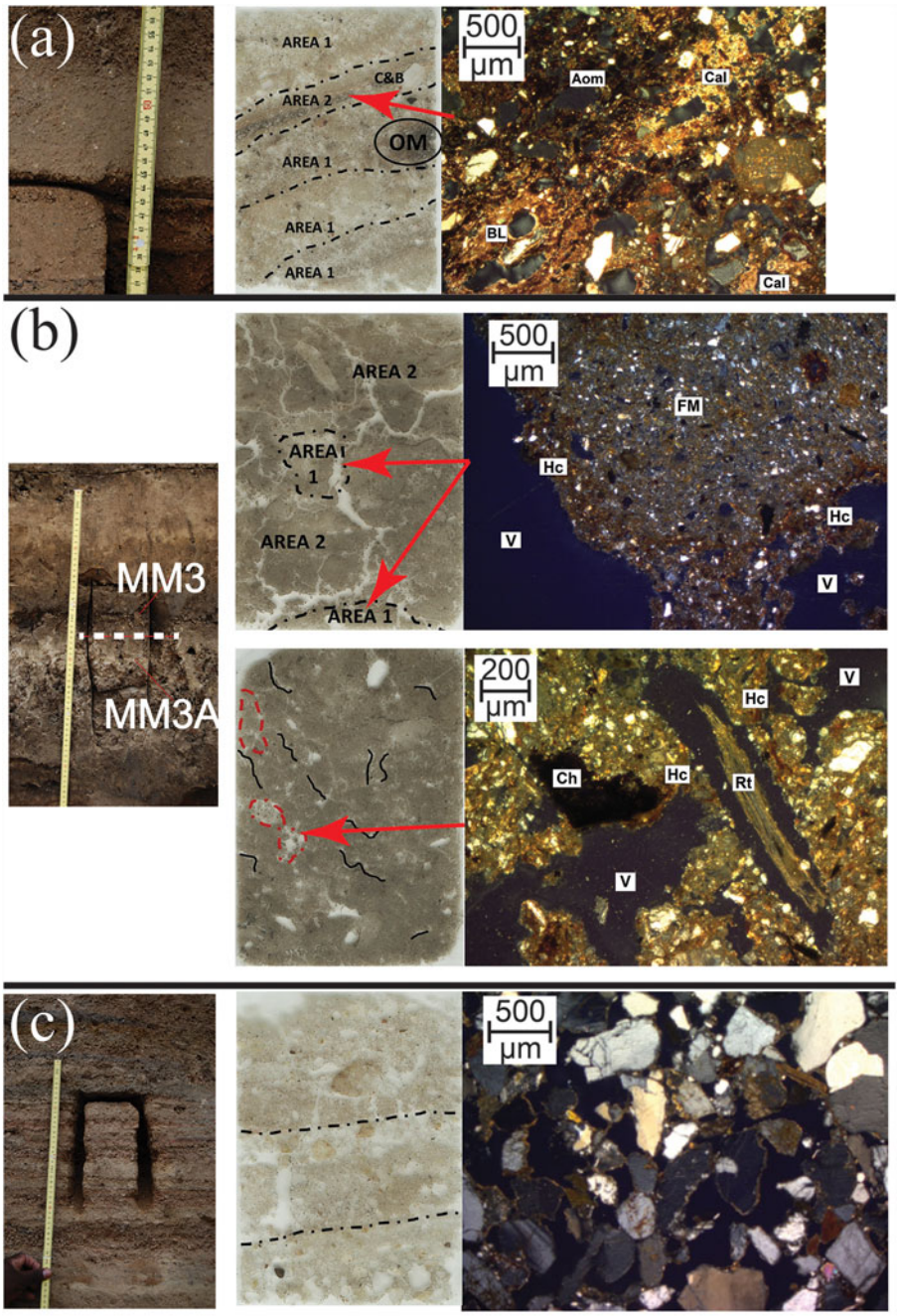

Figure 4. (color online) Location, soil thin sections, and micrographs of the undisturbed soil samples. (a) MM2, micro-laminations indicating variability in the deposition of the sediment and differentiation in composition with Area 1 containing amorphous organic matter (Aom), while Area 2 shows development of calcite coatings and intercalation (Cal), with burnt bone also identified (BL) in the micrograph (cross-polarized light). (b) MM3, a diffused boundary between deposits were identified with (*upper*) Area 1 and Area 2 both show the development of Fe-impregnated hypocoatings (Hc) on large subangular peds, which contain high levels of fine material (FM) and are separated by inter-pedal voids (V; cross-polarized light). (*lower*) Fragments of charcoal (Ch) are displayed in the fine matrix, with the development of Fe- impregnated hypocoating (Hc) on sub-angular peds, while root (Rt) fragments are visible in channel voids (V; cross-polarized light). (c) MM5, microlaminates identified during field observations and weakly identified in thin section, with the groundmass displaying representative quartz coarse material with the development of grano-striations on these coarse fractions from the wetting and drying of clay colloids (cross-polarized light).

Gonné, 2010) and pastoralism, and is maintained as an open, grassy environment.

Off-site samples collected from GRA-1 range from −20.0 to −24.7‰, which indicates predominantly C_3 environments, while the sample collected from ca. 700 cal yr BP was −19.0‰ (~50% C_4). The site is currently vegetated with peanut (*Vigna subterranea*) plants, short grasses, and sparse tree cover and is also used for grazing livestock. The upland swale

https://doi.org/10.1017/qua.2019.25 Published online by Cambridge University Press

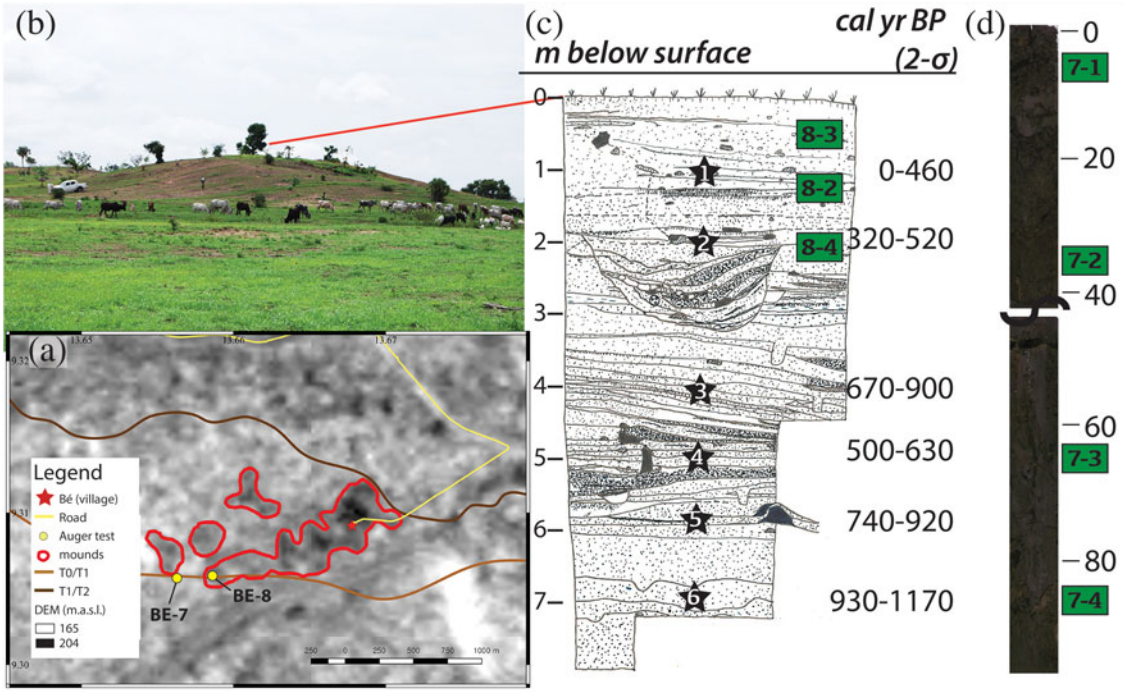

Figure 5. (color online) (a) Mounds at Bé. (b) View of Mound 1 facing east. Photo taken from the location of CAM-Be-Rock 7. (c) Mound 1 excavation digitized from David (1981), showing positions of calibrated radiocarbon ages from Lawn (1973). CAM-Be-Rock 8 samples were collected from the upper 2 m of fill 14.2 m west of David's (1981) Unit 1.

cored locations indicate the presence of a different vegetation regime today than the past. No materials were dated from the auger samples, so it is not presently possible to ascribe a distinct time period to the occurrence of this different vegetation regime. Within environments in the region with relatively low anthropogenic inputs, however, tree cover increases at higher elevations (Stark and Hudson, 1985). The samples analyzed from GRA-1 reflect this pattern.

Within this environment, soil $\delta^{15}N$ values reflect two primary biotic and abiotic processes of the nitrogen cycle.

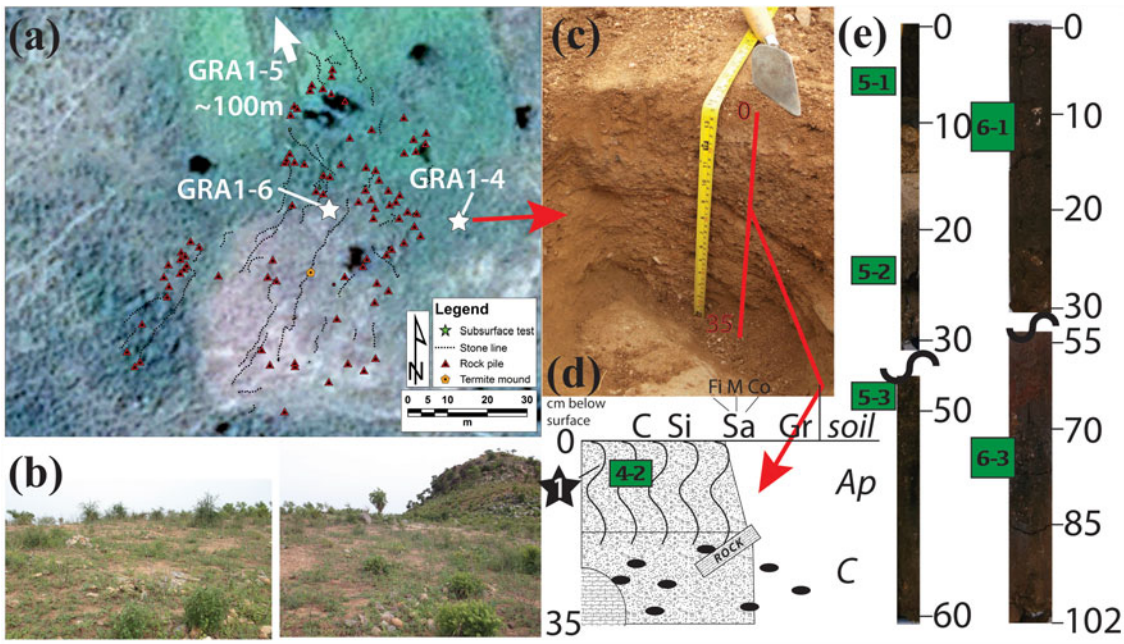

Figure 6. (color online) Fali Mountains site (GRA-1) showing: (a) plan map of site, (b) location of shovel test, (c) photo of excavated shovel test, and (d) profile schematic of shovel test with location of AMS age ISGS A-3309 (680–730 cal yr BP) denoted by a star.

https://doi.org/10.1017/qua.2019.25 Published online by Cambridge University Press

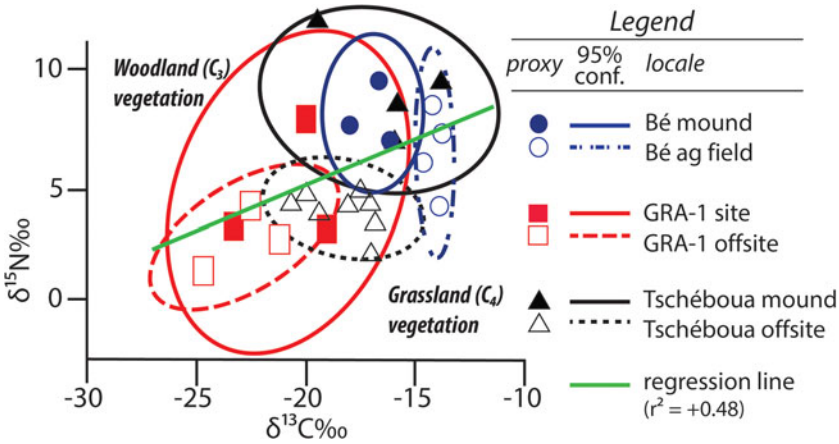

Figure 7. δ^{15}N‰ (vs. AIR) and δ^{13}C‰ (vs. VPDB) for samples collected in on-site (filled shapes) and off-site (open shapes) samples for Bé (blue circles), GRA-1 (red squares), and Langui-Tschéboua (black triangles). Standard ellipses generated in the SIBER package in R (Jackson et al., 2011) at the 95% (2-σ) confidence interval. (For interpretation of the references to color in this figure legend, the reader is referred to the web version of this article.)

High values (Langui-Tschéboua mound, Bé floodplain and mound, and the uppermost sample from the upland swale off-site from GRA-1) are interpreted as ^{15}N-enriched as a result of anthropogenic habitation activities in the case of the former group, and/or dung-enriched soil formation. Lower values from the control samples and upland settings demonstrate comparatively less intensive anthropogenic inputs into the soil. Terraces adjacent to the Langui-Tschéboua mound (TU1, TU2) have common redoximorphic weathering features, which indicate waterlogging and therefore would have been a suboptimal location for sustained human activity.

Interpretation of the stable isotopic data must be considered in the context of the drivers of regional land cover change. Lacustrine proxy data from the Adamaoua Plateau demonstrate that the Late Holocene was a period of overall forest fragmentation relative to the more humid Middle Holocene African Humid Period (AHP), which had denser tree cover (Lebamba et al., 2016). In northern Cameroon and portions of western Africa located at similar latitudes, the termination of the AHP resulted in the expansion of grasslands at the expense of woodlands (Maley and Vernet, 2015). The arrival of farmers and their associated technologies is argued to have corresponded to the expansion of C_4 grasslands associated with this transition (Grollemund et al., 2015). It is also argued that anthropogenic burning encouraged this transition within the context of fragmentation of the Congo rainforest in Central Africa (Garcin et al., 2018).

The results from the Benoué River and Fali Mountains indicate changes in vegetation structure concurrent with intensification of Iron Age settlement and subsistence practices. A phase of apparent rapid mound construction at Langui-Tschéboua appears to correlate with a transition from C_3 to C_4 vegetation and anthropogenic inputs on the site and surrounding landscape. A similar, though less profound change is also indicated at GRA-1. The only sample inferred as corresponding to the occupation of the archaeological site shows the highest δ^{13}C values. Samples from the floodplain of Bé, stratigraphically interpreted as likely relating to the Iron Age and later, demonstrate strong C_4 signatures relative to floodplain soils analyzed from Langui-Tschéboua. After the Iron Age, Langui-Tschéboua appears to have become depopulated and C_3 vegetation returned to the landscape, either through afforestation (Fig. 10) and/or the introduction of non-native C_3 crops. These results signal that, as settlement accelerated at Bé after 1000 yr, more extensive land clearance activities associated with plant and animal cultivation took root. The scale of the transformation captured within the short period (<60 yr) of formation of the Langui-Tschéboua mound suggest the observed transition exceeded the rate of change expected from natural (i.e., orbital) parameters alone. Although there is no available local hydrologic proxy data, regional indicators do not show significant changes in precipitation after 1000 yr (Lézine and Casanova, 1989; Armitage et al., 2015; Lebamba et al., 2016), which reduces the possibility that natural climate changes are responsible for vegetation succession in the Benoué River Valley. Therefore, we interpret human activities associated with land clearance for farming and mound construction as the primary drivers of the change in land cover from the sites of Langui-Tschéboua and Bé.

CONCLUSION

On-site and off-site depositional contexts along the Benoué River Valley and uplands indicate the transition from a C_3 (tree-dominant) to C_4 (grass-dominant) ecological setting in tandem with a phase of rapid mound accumulation. The time-transgressive shift from a C_3 to C_4 environment in the lowlands during the Late Iron Age is not detected at a coevally occupied site in the adjacent Fali Mountains where relatively more C_3 land cover remains. The differing rates of ecological shifts identified from lowland and upland settings appear to

https://doi.org/10.1017/qua.2019.25 Published online by Cambridge University Press

Table 3. Stable $\delta^{15}N$, $\delta^{13}C$ isotopes, and sedimentological context from the Upper Benoué region of northern Cameroon.

Lab number	Field number	Context	Depth (cm below surface); sediment description	Inferred age (yr)*	wt% N	$\delta^{15}N_{AIR}$ (‰)	wt% C	$\delta^{13}C_{VPDB}$ (‰)	Atomic C:N
UIUC001	BE-7-1	Agricultural field next to Bé	3–6; dense clay, no sand	<1000?	0.10	5.5	1.49	−14.6	16.67
UIUC002	BE-7-2	Agricultural field next to Bé	20–23; dense clay, no sand	<1000?	0.07	3.5	1.01	−13.9	17.96
UIUC003	BE-7-3	Agricultural field next to Bé	52–55; dense clay, no sand	<1000?	0.04	7.9	0.57	−14.2	16.69
UIUC004	BE-7-4	Agricultural field next to Bé	83–87; dense clay, some fine silt	<1000?	0.04	6.7	0.61	−13.8	17.65
SNU1	BE-8-2	Bé mound	120–122; silty sand	0–460 (P-1744)	0.06	9.1	0.56	−16.65	10.89
SNU2	BE-8-3	Bé mound	40–42; laminated sand	0–460 (P-1744)	0.12	7.1	1.07	−17.98	10.40
SNU3**	BE-8-4	Bé mound	200; coarse sand	320–520 (P-1557)	0.08	6.4	0.02	−16.13	0.32
UIUC021	GRA1-4-2	GRA-1 subsoil with charcoal and ceramics	9; poorly sorted coarse sand; semi-rounded grains	680–730 (A-3309)	0.04	2.5	0.45	−19.0	13.01
UIUC010	GRA1-5-1	Off-site GRA-1 colluvium	5–8; gritty sandy clay, angular- to rounded-quartz, and feldspar grains	Unknown	0.05	3.5	0.63	−22.5	14.30
UIUC011	GRA1-5-2	Off-site GRA-1 colluvium, but contains wood, grass, charcoal, bone	22–25; massive, poorly sorted, gritty clay-silt	Unknown	0.24	0.8	3.77	−24.7	18.44
UIUC007	GRA1-6-1	Agricultural terrace in GRA-1	9–13; clayey, pelletoidal, silty sand	Unknown	0.08	7.4	1.28	−20.0	18.66
UIUC009	GRA1- 6-3	Agricultural terrace in GRA-1	73–76; gritty, clayey silt, mottled	Unknown	0.05	2.7	1.57	−23.3	34.33
UIUC013	GRA1-5-3	Offsite GRA-1 colluvium	47–51; coarse angular sand and grit in clay matrix	Unknown	0.05	2.2	0.62	−21.2	15.43
UIUC015	LAN-TU1-2	Off-site terrace Langui-Tschéboua	94; very dark brown clay	140 ± 10 (OSL4)	0.07	4.3	1.14	−17.5	20.10
UIUC016	LAN-TU1-3	Off-site terrace Langui-Tschéboua	59; massive fine sand/silty clay	50 ± 10 (OSL3)	0.05	3.5	0.76	−18.1	17.85
UIUC017	LAN-TU1-4	Off-site terrace Langui-Tschéboua	49; fine sandy silty clay/sand, pinhole voids	<50 (OSL3)	0.05	2.8	0.68	−16.8	17.27
UIUC018	LAN-TU1-5	Off-site terrace Langui-Tschéboua	18; fine silty sand, well-sorted; almost no clay	<50 (OSL3)	0.07	4.1	0.97	−20.0	15.33
UIUC019	LAN-TU1-6	Off-site terrace Langui-Tschéboua	3; fine silty sand, well-sorted; slightly more clay	<50 (OSL3)	0.10	3.7	1.34	−20.7	15.13
UIUC028	LAN-TU2-7	Off-site terrace Langui-Tschéboua	56; semi-massive to weak crumb; dark brown silty clay, small percentage sand	<80 (OSL2)	0.05	1.4	0.85	−17.0	18.82
UIUC029	LAN-TU2-8	Off-site terrace Langui-Tschéboua	44; fine sandy silt with weaker crumb structure than UIUC028	<80 (OSL2)	0.06	3.8	0.88	−17.1	18.52
UIUC031	LAN-TU2-10	Off-site terrace Langui-Tschéboua	8; silt/clay with well-sorted fine sand	<80 (OSL2)	0.09	3.2	1.24	−19.4	15.64
UIUC032	LAN-TU3-1	Langui-Tschéboua mound	511; medium/coarse poorly sorted sand; small % silt/clay	5900 ± 400 (OSL7)			0.08	−22.6	
UIUC033	LAN-TU3-2	Langui-Tschéboua mound	480; medium/coarse poorly sorted sand; slightly higher % silt/clay	1100 ± 100 (OSL1)			0.10	−20.5	
UIUC034	LAN-TU3-3	Langui-Tschéboua mound	381; medium/coarse poorly sorted sand; slightly higher % silt/clay	<1100 ± 100 (OSL1), >670–730 (A-3308)	0.07	11.4	0.65	−19.5	11.29
UIUC035	LAN-TU3-4	Langui-Tschéboua mound	328; medium/fine well-sorted silt with voids and root marks	ca. 670–730 (A-3308)	0.06	6.3	1.16	−15.9	21.90
UIUC036	LAN-TU3-5	Langui-Tschéboua mound	307; massive gray ashy fine sandy silt	670–730 (A-3308)	0.05	8.9	1.39	−13.8	34.10

(*Continued*)

Table 3. Continued.

Lab number	Field number	Context	Depth (cm below surface); sediment description	Inferred age (yr)*	wt% N	$\delta^{15}N_{AIR}$ (‰)	wt% C	$\delta^{13}C_{VPDB}$ (‰)	Atomic C:N
UIUC037	LAN-TU3-6	Langui-Tschéboua mound	259; fine silty clay; pinhole voids, termite channels	680–730 (A-3307)			0.24	−16.7	
UIUC038	LAN-TU3-7	Langui-Tschéboua mound	232; fine ashy silt-clay; pinhole voids, charcoal flecks	670–730 (A-3306, A-3307)	0.05	7.9	0.66	−15.8	16.18
UIUC039	LAN-TU3-8	Langui-Tschéboua mound	182; mottled sandy silt/clay; poorly sorted, coarse, rounded sand grains	670–730 (A-3306); *5800 ± 400 (OSL6—discarded)*			0.48	−15.4	
UIUC040	LAN-TU3-9	Langui-Tschéboua mound	99; clayey silt with poorly-sorted subrounded sand grains	<670–730 (A-3306)			0.46	−15.4	
UIUC041	LAN-TU3-10	Langui-Tschéboua mound	8; fine/medium silt with poorly sorted sand grains	<670–730 (A-3306)			0.46	−15.4	
Replicates									
UIUC038	LAN-TU3-7	Langui-Tschéboua mound	232; fine ashy silt-clay; pinhole voids, charcoal flecks	670–730 (A-3306, A-3307)	0.05	8.1	0.66	−15.7	16.20
UIUC039	LAN-TU3-8	Langui-Tschéboua mound	182; mottled sandy silt/clay; poorly sorted coarse rounded sand grains	670–730 (A-3306); *5800 ± 400 (OSL6—discarded)*	0.05	8.0	0.66	−15.8	16.46
UIUC041	LAN-TU3-10	Langui-Tschéboua mound	8; fine/medium silt with poorly sorted sand grains	<670–730 (A-3306)	0.12	6.6	1.77	−19.9	17.26
Average					0.07	5.33	0.89	−17.85	17.03
Standard deviation (1-σ)					0.04	2.68	0.67	2.92	6.28

*For OSL ages, 0 BP = AD 2014. For ^{14}C ages, 0 BP = AD 1950

**Although wt% C is anomalously low, its N concentration and ^{13}C and ^{15}N values are similar to other samples in this study. It is likely that wt %C may have been transcribed incorrectly, but the primary records for the samples were not archived, so we cannot confirm this.

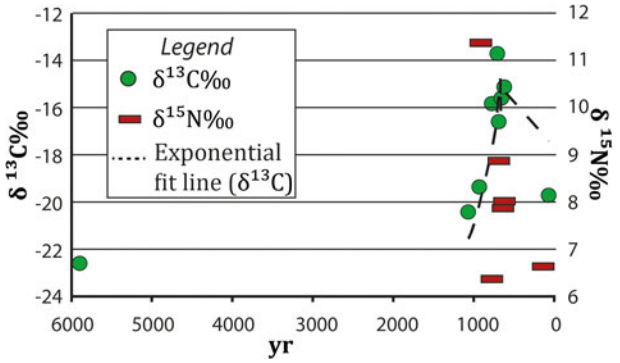

Figure 8. (color online) $\delta^{13}C$ and $\delta^{15}N$ isotopic profile of Langui-Tschéboua. The earlier proxy (5900 yr) is from the underlying alluvial substrate.

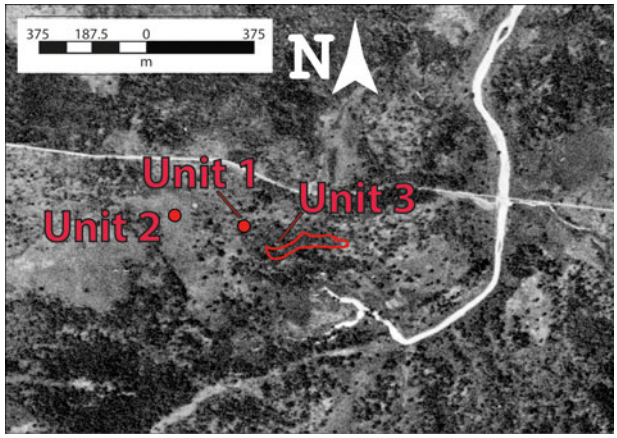

Figure 10. (color online) CORONA satellite image DS1027-1010DA132, taken December 10, 1965 (49 yr on the OSL clock) of Langui-Tschéboua (Fig. 2), with reference to 2014 test units (Wright et al., 2017). The mound location (Unit 3) was vegetated in forest (C_3) at the time of the satellite image. Lateral movement of the river has truncated Iron Age terraces within the last 50 years.

relate to the intensity of archaeological settlements in the different regions. Stable nitrogen isotopes likewise indicate isotopic enrichment of intensively farmed floodplain and mound contexts relative to extensively used landforms with stronger C_3 signatures or soils formed in rapidly aggraded, sandy bed load sediments. Overall, based on the available evidence, we interpret the mound and adjacent floodplains as being the most intensively occupied portions of the Benoué landscape during the Iron Age. Following an inferred regional depopulation and afforestation following the Iron Age, the floodplain has been used more extensively for *karal* agriculture and grazing.

Although the observed environmental variation is based on a limited isotopic dataset, these data demonstrate the potential for prehistoric human settlement practices to alter endemic ecological systems rapidly and profoundly and exploit different plant communities at different times. There is mounting evidence that land burning and clearance was substantial during the Iron Age and sufficient to alter local ecologies (Bayon et al., 2012; Morin-Rivat et al., 2014; Kay and Kaplan, 2015). There is considerable debate, however, about whether forest fragmentation occurred prior to or concurrent with the spread of farmers across Central Africa (Maley, 2002; Lézine et al., 2013; Bostoen et al., 2015). Our data suggests that as land settlement activities (e.g., mound construction) intensified, there was a concomitant shift to a C_4 savanna ecosystem. If this pattern bears out across the region, there are significant implications for the nature of domestication of African landscapes and the degree to which humans and their domesticates are interdependent. As the scale and scope of the human footprint increases across the planet, biodiversity in all its forms must be quantified and contextualized to better understand sustainability in landscape processes.

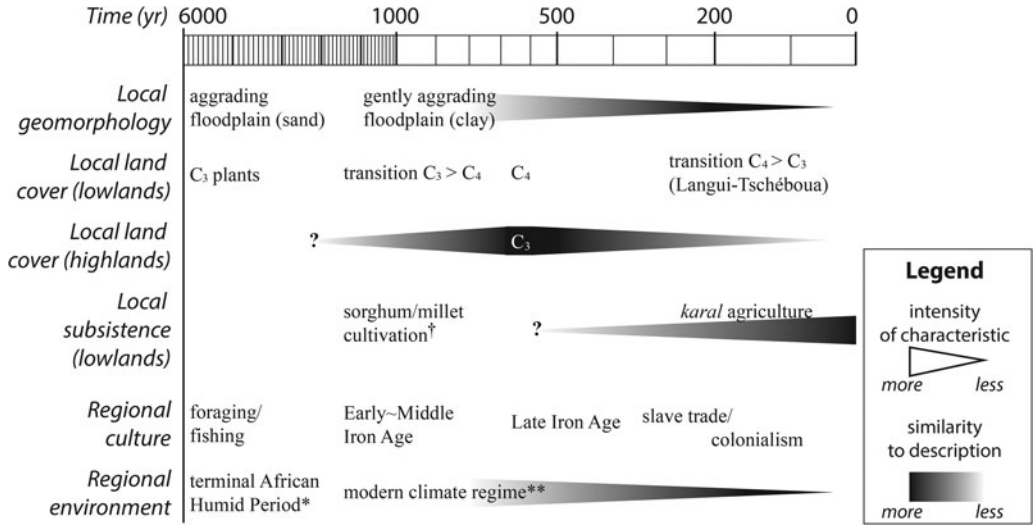

Figure 9. Local and regional human ecologies relative to the Benoué River floodplain, northern Cameroon. Data sources: †, David (1981); *, Armitage et al. (2015) and Lézine and Casanova (1989); **, Lebamba et al. (2016) and Armitage et al. (2015).

https://doi.org/10.1017/qua.2019.25 Published online by Cambridge University Press

ACKNOWLEDGMENTS

Permission to conduct this research project was granted by Ministère de la Recherche Scientifique et de l'Innovation in Cameroon. A National Geographic Committee for Research and Exploration grant (9404-13) and Seoul National University faculty research grant funded the fieldwork and sample analyses. We would particularly like to thank the Lamido of Bé, Abdurahman Aman Saly, and the Lawan of Langui for their assistance and support. We would also like to thank our field assistants Kankaou Dirna and Haman Oumarou for help in preparing the sections for profiling at Langui-Tschéboua. George MacLeod at the University of Stirling, Scotland, prepared the thin sections for micromorphological analysis. We thank Ling Xue (Northwest University, Xi'an, China), for preparing soil samples for isotopic analysis in the Department of Anthropology Environmental Isotope Paleobiogeochemistry Laboratory, University of Illinois. Seoyoung Huh at the Korea Basic Science Institute assisted in preparing and running the OSL samples. We also wish to thank four anonymous reviewers, associate editor J. Tyler Faith, and senior editor Derek Booth for constructive comments to improve the quality of the manuscript.

SUPPLEMENTARY MATERIAL

The supplementary material for this article can be found at https://doi.org/10.1017/qua.2019.25.

REFERENCES

Ackermann, O., Greenbaum, N., Bruins, H., Porat, N., Bar-Matthews, M., Almogi-Labin, A., Schilman, B., *et al*., 2014. Palaeoenvironment and anthropogenic activity in the southeastern Mediterranean since the mid-Holocene: the case of Tell es-Safi/Gath, Israel. *Quaternary International* 328–329, 226–243.

Aitken, M.J., 1998. *An Introduction to Optical Dating: The Dating of Quaternary Sediments by the Use of Photon-Stimulated Luminescence*. Oxford University Press, Oxford.

Ambrose, S.H., 1991. Effects of diet, climate and physiology on nitrogen isotope abundances in terrestrial foodwebs. *Journal of Archaeological Science* 18, 293–317.

Ambrose, S.H., 2010. Coevolution of composite-tool technology, constructive memory, and language: implications for the evolution of modern human behavior. *Current Anthropology* 51, S135–S147.

Ambrose, S.H., Sikes, N.E., 1991. Soil carbon isotope evidence for Holocene habitat change in the Kenya Rift Valley. *Science* 253, 1402–1405.

Armitage, S.J., Bristow, C.S., Drake, N.A., 2015. West African monsoon dynamics inferred from abrupt fluctuations of Lake Mega-Chad. *Proceedings of the National Academy of Sciences of the United States of America* 112, 8543–8548.

Bayon, G., Dennielou, B., Etoubleau, J., Ponzevera, E., Toucanne, S., Bermell, S., 2012. Intensifying weathering and land use in Iron Age Central Africa. *Science* 335, 1219–1222.

Boivin, N.L., Zeder, M.A., Fuller, D.Q., Crowther, A., Larson, G., Erlandson, J.M., Denham, T., Petraglia, M.D., 2016. Ecological consequences of human niche construction: examining long-term anthropogenic shaping of global species distributions. *Proceedings of the National Academy of Sciences of the United States of America* 113, 6388–6396.

Bostoen, K., Clist, B., Doumenge, C., Grollemund, R., Hombert, J.-M., Muluwa, J.K., Maley, J., 2015. Middle to Late Holocene paleoclimatic change and the early Bantu expansion in the rain forests of western Central Africa. *Current Anthropology* 56, 354–384.

Bullock, P., Federoff, N., Jongerius, A., Stoops, G., Turina, T., Babel, U., 1985. *Handbook for Soil Thin Section Description*. Waine Research Publications, Wolverhampton.

Clist, B., Bostoen, K., de Maret, P., Eggert, M.K.H., Höhn, A., Mbida Mindzié, C., Neumann, K., Seidensticker, D., 2018. Did human activity really trigger the late Holocene rainforest crisis in Central Africa? *Proceedings of the National Academy of Sciences of the United States of America* 115, E4733.

Commisso, R.G., Nelson, D.E., 2006. Modern plant $\delta^{15}N$ values reflect ancient human activity. *Journal of Archaeological Science* 33, 1167–1176.

Crowther, A., Prendergast, M.E., Fuller, D.Q., Boivin, N., 2018. Subsistence mosaics, forager-farmer interactions, and the transition to food production in eastern Africa. *Quaternary International* 489, 101–120.

David, N., 1968. Archaeological reconnaissance in Cameroon. *Expedition* 10, 21–31.

David, N., 1981. The archaeological background of Cameroonian history. In: Tardits, C. (Ed.), *Contribution de la recherche ethnologique a l'histoire des civilisations du Camerouns*. Colloques Internationaux du Centre National de la Recherche Scientifique. Editions du CNRS, Paris, pp. 79–98.

Delègue, M.-A., Fuhr, M., Schwartz, D., Mariotti, A., Nasi, R., 2001. Recent origin of a large part of the forest cover in the Gabon coastal area based on stable carbon isotope data. *Oecologia* 129, 106–113.

Foley, S.F., Gronenborn, D., Andreae, M.O., Kadereit, J.W., Esper, J., Scholz, D., Pöschl, U., *et al*., 2013. The Palaeoanthropocene—the beginnings of anthropogenic environmental change. *Anthropocene* 3, 83–88.

Galbraith, R.F., Roberts, R.G., 2012. Statistical aspects of equivalent dose and error calculation and display in OSL dating: an overview and some recommendations. *Quaternary Geochronology* 11, 1–27.

Galbraith, R.F., Roberts, R.G., Laslett, G.M., Yoshida, H., Olley, J.M., 1999. Optical dating of single and multiple grains of quartz from Jinmium rock shelter, northern Australia: part I, experimental design and statistical models. *Archaeometry* 41, 339–364.

Garcin, Y., Deschamps, P., Ménot, G., de Saulieu, G., Schefuß, E., Sebag, D., Dupont, L.M., *et al*., 2018. Early anthropogenic impact on Western Central African rainforests 2,600 y ago. *Proceedings of the National Academy of Sciences of the United States of America* 115, 3261–3266.

Gonné, B., 2010. Karal land: family cultural patrimony or a commercialized product on the Diamaré Plain. In: Anseeuw, W., Alden, C. (Eds.), *The Struggle Over Land in Africa. Conflicts, Politics and Change*. Human Sciences Research Council Press, Cape Town, pp. 71–82.

Grollemund, R., Branford, S., Bostoen, K., Meade, A., Venditti, C., Pagel, M., 2015. Bantu expansion shows that habitat alters the route and pace of human dispersals. *Proceedings of the National Academy of Sciences of the United States of America* 112, 13296–13301.

Högberg, P., 1997. Tansley Review No. *95: ^{15}N natural abundance in soil-plant systems.* New Phytologist 137, 179–203.

Jackson, A.L., Inger, R., Parnell, A.C., Bearhop, S., 2011. Comparing isotopic niche widths among and within communities: SIBER – Stable Isotope Bayesian Ellipses in R. *Journal of Animal Ecology* 80, 595–602.

Kahlheber, S., Neumann, K., 2007. The development of plant cultivation in semi-arid West Africa. In: Denham, T.P., Iriarte, J., Vrydaghs, L. (Eds.), *Rethinking Agriculture: Archaeological and Ethnoarchaeological Perspectives*. Left Coast Press, Walnut Creek, California, pp. 320–346.

Kay, A.U., Kaplan, J.O., 2015. Human subsistence and land use in sub-Saharan Africa, 1000 BC to AD 1500: a review, quantification, and classification. *Anthropocene* 9, 14–32.

Kenga, R., Njoya, A., M'biandoum, M., 2005. Analysis of constraints to agricultural production in the Sudano Savanna zone of Cameroon and implication for research priority setting. *Tropicultura* 23, 91–99.

Killick, D., 2015. Invention and innovation in African iron-smelting technologies. *Cambridge Archaeological Journal* 25, 307–319.

Kim, S.-T., Coplen, T.B., Horita, J., 2015. Normalization of stable isotope data for carbonate minerals: implementation of IUPAC guidelines. *Geochimica et Cosmochimica Acta* 158, 276–289.

Kohn, M.J., 2010. Carbon isotope compositions of terrestrial C3 plants as indicators of (paleo)ecology and (paleo)climate. *Proceedings of the National Academy of Sciences of the United States of America* 107, 19691–19695.

Lander, F., Russell, T., 2018. The archaeological evidence for the appearance of pastoralism and farming in southern Africa. *PLOS ONE* 13, e0198941.

Lawn, B., 1973. University of Pennsylvania radiocarbon dates XV. *Radiocarbon* 15, 367–381.

Lebamba, J., Vincens, A., Lézine, A.-M., Marchant, R., Buchet, G., 2016. Forest-savannah dynamics on the Adamawa plateau (Central Cameroon) during the "African humid period" termination: a new high-resolution pollen record from Lake Tizong. *Review of Palaeobotany and Palynology* 235, 129–139.

Lézine, A.M., Casanova, J., 1989. Pollen and hydrological evidence for interpretation of past climates in tropical Africa during the Holocene. *Quaternary Science Reviews* 8, 45–55.

Lézine, A.-M., Holl, A.F.C., Lebamba, J., Vincens, A., Assi-Khaudjis, C., Février, L., Sultan, É., 2013. Temporal relationship between Holocene human occupation and vegetation change along the northwestern margin of the Central African rainforest. *Comptes Rendus Geoscience* 345, 327–335.

MacEachern, S., 2012. The Holocene history of the southern Lake Chad Basin: archaeological, linguistic and genetic evidence. *African Archaeological Review* 29, 1–19.

Maley, J., 2002. A catastrophic destruction of African forests about 2,500 years ago still exerts a major influence on present vegetation formations. *IDS Bulletin* 33, 13–30.

Maley, J., Giresse, P., Doumenge, C., Favier, C., 2012. Comment on "Intensifying Weathering and Land Use in Iron Age Central Africa." *Science* 337, 1040.

Maley, J., Vernet, R., 2015. Populations and climatic evolution in north tropical Africa from the end of the Neolithic to the dawn of the modern era. *African Archaeological Review* 32, 179–232.

Manning, K., Pelling, R., Higham, T., Schwenniger, J.-L., Fuller, D.Q., 2011. 4500-year old domesticated pearl millet (Pennisetum glaucum) from the Tilemsi Valley, Mali: new insights into an alternative cereal domestication pathway. *Journal of Archaeological Science* 38, 312–322.

Marchant, R., Richer, S., Boles, O., Capitani, C., Courtney-Mustaphi, C.J., Lane, P., Prendergast, M.E., *et al*., 2018. Drivers and trajectories of land cover change in East Africa: human and environmental interactions from 6000 years ago to present. *Earth-Science Reviews* 178, 322–378.

Marshall, F., Reid, R.E.B., Goldstein, S., Storozum, M., Wreschnig, A., Hu, L., Kiura, P., Shahack-Gross, R., Ambrose, S.H., 2018. Ancient herders enriched and restructured African grasslands. *Nature* 561, 387–390.

Meharg, A.A., Deacon, C., Edwards, K.J., Donaldson, M., Davidson, D.A., Spring, C., Scrimgeour, C.M., Feldmann, J., Rabb, A., 2006. Ancient manuring practices pollute arable soils at the St Kilda World Heritage Site, Scottish North Atlantic. *Chemosphere* 64, 1818–1828.

Morin-Rivat, J., Fayolle, A., Gillet, J.-F., Bourland, N., Gourlet-Fleury, S., Oslisly, R., Bremond, L., Bentaleb, I., Beeckman, H., Doucet, J.-L., 2014. New evidence of human activities during the Holocene in the lowland forests of the northern Congo Basin. *Radiocarbon* 56, 209–220.

Murray, A.S., Wintle, A.G., 2000. Luminescence dating of quartz using an improved single-aliquot regenerative-dose protocol. *Radiation Measurements* 32, 57–73.

Murray, A.S., Wintle, A.G., 2003. The single aliquot regenerative dose protocol: potential for improvements in reliability. *Radiation Measurements* 37, 377–381.

Natelhoffer, K.J., Fry, B., 1988. Controls on natural nitrogen-15 and carbon-13 abundances in forest soil organic matter. *Soil Science Society of America Journal* 52, 1633–1640.

O'Leary, M.H., 1988. Carbon isotopes in photosynthesis. *BioScience* 38, 328–336.

Olley, J.M., Murray, A., Roberts, R.G., 1996. The effects of disequilibria in the uranium and thorium decay chains on burial dose rates in fluvial sediments. *Quaternary Science Reviews* 15, 751–760.

Oslisly, R., White, L., Bentaleb, I., Favier, C., Fontugne, M., Gillet, J.-F., Sebag, D., 2013. Climatic and cultural changes in the west Congo Basin forests over the past 5000 years. *Philosophical Transactions of the Royal Society B: Biological Sciences* 368, 20120304.

Prescott, J.R., Hutton, J.T., 1994. Cosmic ray contributions to dose rates for luminescence and ESR dating: large depths and long-term time variations. *Radiation Measurements* 23, 497–500.

Qi, H., Coplen, T.B., Mroczkowski, S.J., Brand, W.A., Brandes, L., Geilmann, H., Schimmelmann, A., 2016. A new organic reference material, l-glutamic acid, USGS41a, for $\delta^{13}C$ and $\delta^{15}N$ measurements – a replacement for USGS41. *Rapid Communications in Mass Spectrometry* 30, 859–866.

Reimer, P.J., Bard, E., Bayliss, A., Beck, J.W., Blackwell, P.G., Bronk Ramsey, C., Buck, C.E., *et al*., 2013. IntCal13 and Marine13 radiocarbon age calibration curves 0–50,000 years cal BP. *Radiocarbon* 55, 1869–1887.

Ruddiman, W.F., 2013. The Anthropocene. *Annual Review of Earth and Planetary Sciences* 41, 45–68.

Runge, J., 2002. Holocene landscape history and palaeohydrology evidenced by stable carbon isotope ($\delta^{13}C$) analysis of alluvial sediments in the Mbari valley (5 degrees N/23 degrees E), Central African Republic. *Catena* 48, 67–87.

Russell, T., Silva, F., Steele, J., 2014. Modelling the spread of farming in the Bantu-speaking regions of Africa: an archaeology-based phylogeography. *PLoS ONE* 9, e87854.

Schoeneberger, P.J., Wysocki, D.A., Benham, E C., Soil Survey Staff, 2012. *Field Book for Describing and Sampling Soils, Version 3.0*. Natural Resources Conservation Service, National Soil Survey Center, Lincoln.

Shahack-Gross, R., Simons, A., Ambrose, S.H., 2008. Identification of pastoral sites using stable nitrogen and carbon isotopes from bulk sediment samples: a case study in modern and

archaeological pastoral settlements in Kenya. *Journal of Archaeological Science* 35, 983–990.

Solís-Castillo, B., Golyeva, A., Sedov, S., Solleiro-Rebolledo, E., López-Rivera, S., 2015. Phytoliths, stable carbon isotopes and micromorphology of a buried alluvial soil in Southern Mexico: a polychronous record of environmental change during Middle Holocene. *Quaternary International* 365, 150–158.

Stark, M.A., Hudson, R.J., 1985. Plant communities' structure in Benoue National Park, Cameroon: a cluster association analysis. *African Journal of Ecology* 23, 21–27.

Stoops, G., 2003. *Guidelines for Analysis and Description of Soil and Regolith Thin Sections*. Soil Science Society of America, Madison.

Stuiver, M., Reimer, P.J., Reimer, R.W., 2019. CALIB 7.1 (accessed January 7, 2019). http://calib.org.

Wang, L., D'Odorico, P., Ries, L., Macko, S.A., 2010. Patterns and implications of plant-soil $\delta^{13}C$ and $\delta^{15}N$ values in African savanna ecosystems. *Quaternary Research* 73, 77–83.

White, F., 1983. *The Vegetation of Africa: A Descriptive Memoir to Accompany the UNESCO/AETFAT/UNSO Vegetation Map of Africa*. United Nations Educational and Scientific Cultural Organization, Paris.

WoldeGabriel, G., Ambrose, S.H., Barboni, D., Bonnefille, R., Bremond, L., Currie, B., DeGusta, D., *et al*., 2009. The geological, isotopic, botanical, invertebrate, and lower vertebrate surroundings of *Ardipithecus ramidus*. *Science* 326, 65e1–65e5.

Wright, D.K., MacEachern, S., Choi, J., Choi, J.H., Lang, C., Djoussou, J.-M.D., 2017. Iron Age landscapes of the Benue River Valley, Cameroon. *Journal of Field Archaeology* 42, 394–407.

https://doi.org/10.1017/qua.2019.25 Published online by Cambridge University Press